Permafrost and Periglacial Processes

WILEY

RESEARCH ARTICLE OPEN ACCESS

Experimental Investigation of Moisture Movement During Freeze–Thaw Cycles and Its Effect on Physical Rock Weathering in Low-Porosity Alpine Limestone

Andrew Mitchell | Oliver Sass

Department of Geography, University of Bayreuth, Bayreuth, Germany

Correspondence: Andrew Mitchell (andrew.mitchell@uni-bayreuth.de)

Received: 6 October 2025 | **Revised:** 27 February 2026 | **Accepted:** 17 March 2026

Keywords: acoustic emissions | freeze–thaw | ice segregation | limestone | rock moisture | rock weathering

ABSTRACT

The progressive weakening of alpine rockwalls through subcritical cracking, driven by repeated low-magnitude stress processes, plays a key role in alpine rock weathering. Laboratory studies using acoustic emission (AE) monitoring have shown that thermal stresses from freeze–thaw cycling induce crack propagation, with recent work highlighting the influence of rock moisture saturation. However, the role of moisture availability and movement within the outer rockwall remains poorly constrained. To address this gap, we conducted laboratory experiments on 40 × 20 × 20 cm samples of Wetterstein limestone (Northern Calcareous Alps), using AE sensors to track subcritical cracking during repeated diurnal and 72-h freeze–thaw cycles between 7°C and −8°C. Initial rock moisture saturation was varied across runs, and moisture redistribution was monitored via electrical resistance measurements. Our results show that while higher saturation generally enhances rock weathering, maximum crack intensity occurs at 70%–75% saturation, challenging the assumption that > 91% saturation represents optimal conditions. Among moisture-driven processes, volumetric expansion produced the highest weathering intensities (but for a shorter period of time), whereas ice segregation generated greater cumulative subcritical cracking due to the longer duration. Based on these findings and evidence of ice segregation, we propose a refined frost cracking window of −4°C to −9°C for Wetterstein limestone. These insights advance our understanding of the coupled role of rock moisture and temperature in alpine rockwall preconditioning for rockfall, though further work is needed to assess the impact of wet-dry weathering during freeze–thaw cycles and the role of increased surface moisture availability.

1 | Introduction

In alpine rockwalls, erosion caused by rockfall is a key part of the geomorphic landscape evolution [1] and a natural hazard to people and infrastructure in the mountains [2]. While rockfall is the end result of critical cracking, the preconditioning and weakening of the overall rockwall by repeated low-magnitude processes creating stresses below the critical pressure, so-called subcritical or microcracking [3, 4], are key agents of mechanical rockwall weakening. Eppes [5] hypothesise that subcritical crack tip propagation is down to stress intensity and crack tip chemical reactions, with environmental conditions such as temperature and moisture availability controlling the cracking rates independently of overall stress loading magnitude.

Many studies have shown different weathering process dependence on temperature stresses [6–9], but increasingly rock moisture is seen to be a critical weathering agent [2, 10–14]. This is because dynamic temperature regimes not only cause thermal stresses [15] but also lead to rock moisture migration/movement [16]. This movement alone can cause buildup of hydrostatic pressures in crack tips [17, 18]. Wetting/drying is

https://doi.org/10.1002/ppp.70035

also another important rockwall stressor by respectively causing swelling and shrinking of the rock [19] and synergistically creating thermal stresses in the drying process [11]. In alpine rockwalls, frost cracking is considered the main driving stress mechanism of rockwall breakdown in the alps [20–22], causing both subcritical and critical cracking [23]. Frost cracking weathering processes include both volumetric expansion (VE) and ice segregation (IS) [24], which have been shown to produce ice pressures of up to 207 and 30 MPa respectively [22, 25], exceeding the tensile strength of most rocks [26], including Wetterstein limestone [15], granite [26] and gneiss [27]. The stress from VE is caused by a 9% increase in volume of in situ pore water when it freezes during rapid freezing cycles [28], and if rock moisture expelled by the rapid ice formation cannot find another pore to escape to due to poor interconnection, hydraulic pressures can increase in the surrounding porosity [17]. Walder and Hallet [29] find that VE favours rock moisture saturation $>91\%$, and Matsuoka [28] suggests a value around 80%, dependent on lithology. This rock moisture saturation is rarely found in natural rockwalls [30] and as Jia et al. [31] found, nonuniformly sized pore structure can lead to crack propagation if only a portion of the pore space is saturated.

IS meanwhile favours more sustained freezing periods when unfrozen rock moisture migrates towards the frozen fringe by induced temperature gradients or cryosuction [32]. This moisture movement in the frozen rock pores is facilitated by the fact that a thin water film, <9 nm, remains between the pore walls and ice crystals [33–35]. Stresses from IS are built up by continued expansion of the ice lens and crystallisation pressures [36] and a buildup of hydrostatic pressures at the frozen fringe [37] caused by the thermodynamic potential gradient–driven moisture movement [32]. Consequently, for frost weathering, rock moisture presence and availability are prerequisite [38] and understanding moisture movement during these temperature cycles is critical.

Mechanical weathering processes and associated subcritical crack propagation or microcracking [5] have been examined by several studies using acoustic emission (AE) sensors [7]. The rapid release of energy caused by crack nucleation creates transient elastic waves or AEs [39]. The resulting surface movement caused by these waves can be detected by AE sensors, with high sensitivity in the low ultrasonic frequency range [40], amplified and converted into discrete electrical signals [41]. The location of the origin of these AEs can be determined based on material dependent wave velocity and arrival times between different sensors [40]. Freezing experiments with stable boundary conditions were investigated using AEs as a weathering proxy in several studies [10, 25, 27] and in more natural dynamic thermal boundary conditions by Maji and Murton [40] and Mayer et al. [42]. While these studies acknowledge the importance of rock moisture in different lithologies, the distribution and movement at depth of it during freeze–thaw cycles are not measured. In response to this, an earlier study by Mitchell and Sass [11] focused specifically on the effects of varying rock moisture to physical rock weathering. The study found that there were marked differences in when subcritical cracking occurred and the intensity with which it occurred in various climatic weathering conditions in relation to moisture content. The greatest weathering effect and most pronounced overall difference related to moisture saturation was seen in freeze–thaw cycles. In this case, the higher saturated samples showed a much greater weathering potential. It was also hypothesised that the availability of rock moisture is at least as important as the initial rock moisture in that area, a suggestion also made by Mayer et al. [10]. Building on these earlier investigations, the main objectives of our freeze–thaw weathering laboratory study are to determine:

1. does increased rock moisture saturation lead to increased rock weathering efficacy and what is the role of rock moisture availability in freeze–thaw cycles?
2. how do different rock moisture movement processes affect the efficacy of subcritical cracking?
3. what is the effect of freeze–thaw cycle length on different rock moisture conditions?
4. can the findings from Points 1–3 be transferred to natural rockwalls and how does this advance our understanding of frost weathering in Arctic and Alpine regions?

2 | Materials and Methods

2.1 | Samples

As the field sites in the ClimRock project are located in the Northern Calcereous Alps near the German-Austrian border, a block of Wetterstein Limestone typical of the area was used for the laboratory experiments. This was extracted from Hafnach quarry by Flintsbach, Bavaria, and samples were sawn from this same block to ensure similar stress history. Upon arrival at the University of Bayreuth, the samples were stored in a room with an average temperature of 18.93°C ± 0.59°C and average humidity of 75.51% ± 6.02%.

For this series of experiments, two rock samples of 20 cm × 20 cm × 40 cm were used. This sample size was chosen to simulate the outer 40 cm of rockwall, which shows highest rock moisture fluctuation [2], and be inside weight and size restrictions for our climate chamber (Kambic KK-340 CHLT). For each experiment, the block's starting moisture content was controlled by weight. Oven-drying at 60°C until weight change stops was used to determine 0% saturation sample weight. This temperature was used to remove the free water in the sample while not causing excessive thermal stress. Gradual submersion in deionised water was used to saturate samples. When no further weight change was observed, the sample was considered saturated. The pre-experiment rock sample effective porosity range was 0.76% to 0.61% (seen in Figure 1a). Figure 1b shows electrical conductance at depth for fully saturated samples at 20°C. The variation seen implies greater effective porosity at depth in sample RS1 compared with RS2.

2.2 | Experiment Procedure

Our experimental setup was a continuation from earlier work by Mayer et al. [10] and Mitchell and Sass [11]. While Mayer et al. [10] focused on the effect of temperature on frost cracking efficacy in single long freezing cycles and Mitchell and Sass [11] looked at

(a)

Samples	Experiments	Effective Porosity (%)	Increase (%)
RS1	pre-exp.	0.76	1.64
	post (exp.50, exp.60)	0.78	
RS2	pre-exp.	0.61	2.06
	post (exp.70, exp.75)	0.62	

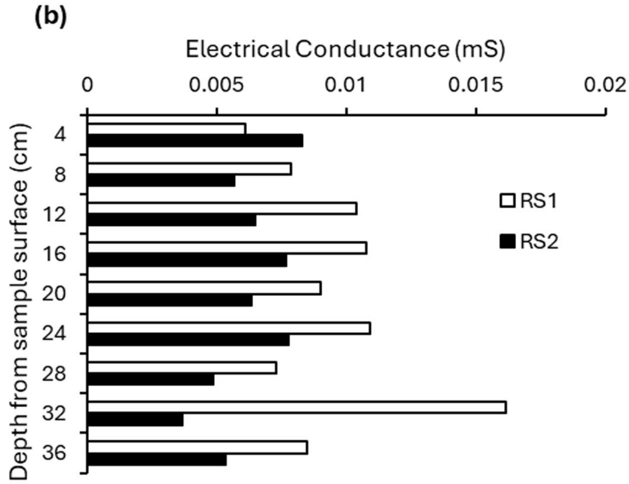

FIGURE 1 | (a) Effective porosities of samples before and after different experiment runs. (b) Sample porosity distribution based on electrical conductance.

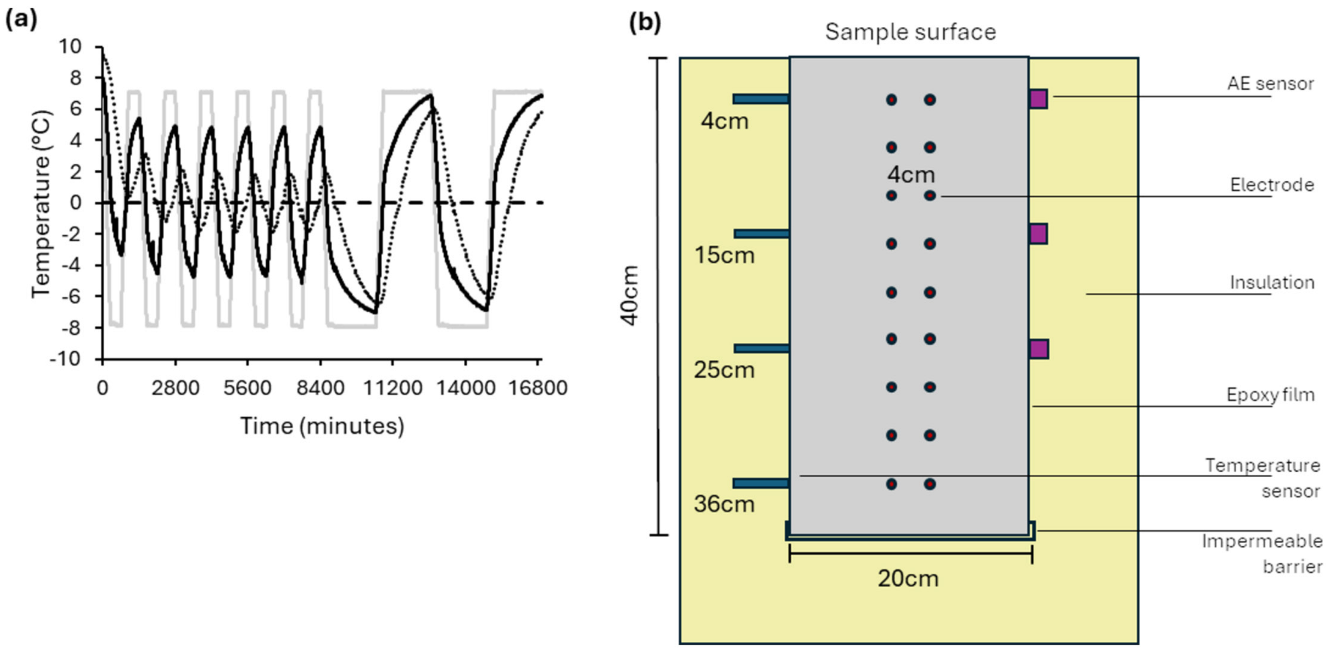

FIGURE 2 | Experiment setup including (a) air temperature cycles over the course of an experiment (grey line), rock temperature at 0 cm (solid black) 40 cm (dotted black) from sample surface. 0°C temperature is highlighted by the dashed line. (b) 2D schematic of experiment setup with instrument locations.

the effect of total rock moisture on different weathering regimes in Wetterstein limestone, now, the emphasis is on how different moisture movement processes affect weathering in a series of diurnal and multiday freeze–thaw temperature cycles (Figure 2a). Average starting moisture saturation (%) of the rock sample at the start of the experiment was used to name the four experiment runs: exp.75, exp.70, exp.60 and exp.50. The samples used for each saturation and their effective porosity can be seen in Figure 1a.

The rock samples had a submillimetre layer of epoxy resin applied to the sides of the sample. This was to prevent lateral rock moisture infiltration, while still maintaining permeability from the surface and base. For each experiment run, the samples were saturated by immersion to the desired weight. The base was then sealed with clingfilm to create an impermeable barrier so that moisture was not lost from the base of the sample during the cycles. The samples were placed in a climate chamber (Kambič KK-340 CHLT, < ± 0.3°C) with the top exposed to the air and the sides and base surrounded with a minimum of 6 cm XPS foam insulation (Figure 2b). Each sample was cooled towards the starting cycle temperature of 7°C for 24 h. For six ca. 24-h cycles (1400 min) and then two longer ca. 72 h (4280 min) cycles, the air temperature cycled between 7°C and −8°C at a gradient of 3°C per hour, reflecting potential ranges of freeze–thaw cycles seen in the Northern Alps. The rock temperature was monitored at 1 min resolution using Greisinger Pt 1000 temperature sensors (0.03°C accuracy) at 4, 15, 25 and 36 cm depth (laterally in the sample centre). To monitor rock moisture, nine electrode pairs were inserted at 4 to 36 cm from surface with even spacing. The individual electrode pairs had a 4-cm spacing and consisted of 6 mm brass expansion plugs with stainless steel bolts inserted to 1 mm below the rock surface. The Resistance Logger was produced internally at University of Bayreuth and can register a maximum resistance of 2,048,000 Ohm in 15.625 Ohm steps at 1 µA with a gain error of 0.05%–0.35% and recorded data at 1-min intervals.

To monitor fracture propagation, we installed three Physical Acoustics PK61 AE sensors with a 35–65-kHz frequency range at the side of the sample using a thin layer of acryl at 4, 15 and 25 cm from the sample surface. AE signals were recorded using a µSHM node from Physical Acoustics with near constant sampling (10 K/s). We had initially hoped to use a fourth AE sensor at 36 cm from the surface, but unfortunately, it broke during the experiments due to moisture damage.

2.3 | Electrical Conductance

In porous solids, such as Wetterstein limestone, electrical conductance (or resistance) is largely dependent on the rock's moisture content [43]. Consequently, it can be used to estimate rock moisture saturation and its variation over time. Conductance is also dependent on temperature and the presence of soluble salts such as NaCl or CaS04 [13]. The latter can affect results by factors of > 10 [44]; fortunately, however, the Wetterstein limestone used in this study is largely free of soluble salts, and so this is less of an issue.

While electrical resistance is recorded by our sensors, the relation of conductance is more intuitive to moisture content in rock [45], and so converted using the below relation:

$$G = 1/R$$

where G is conductance in siemens (S) and R is resistance in ohm (Ω).

2.3.1 | Temperature Correction

To model temperature (T) at a specific depth (n) and time (t), we used the below equation (after [10]), where the temperature measured by the temperature gauge is TL and the gradient between the two given sensors is TG.

$$T(n,t) = \mathrm{TL}(t) + n \cdot \mathrm{TG}(t), 0 \leq n \leq 40\,\mathrm{cm}$$

From this modelled temperature data, we then calibrated for the temperature dependency of resistance measurements. To create a Wetterstein limestone–specific temperature correction, five 10 cm^3 samples, from the same block as our experiment samples, were saturated by immersion and brought to 20°C and 5°C in a climate chamber and resistance readings recorded. The linear correlation between these two temperatures showed that to adjust the conductance relative to 20°C (G), a correction using the below equation is required:

$$G = \mathrm{Graw} + (20 - T) \cdot 6.2\mathrm{e} - 08$$

where Graw is the measured conductance, T is the modelled temperature at that depth and 6.2e−08 is the correction factor. This linear correction is applied to the full temperature range of the experiment.

2.4 | Saturation Model

To create a Wetterstein limestone–specific electrical conductance to VWC (%) model, five 10 cm^3 samples, from the same block as our experiment samples, were saturated by immersion from 100% to 30% in steps of 10% and the volumetric water content calculated by weight change. For each saturation step, the samples were wrapped in clingfilm to maintain moisture content and placed in a climate chamber at 20°C. Once the centre of the sample had reached, the target temperature electrical conductance was recorded for 1 h with a pair of electrodes at 4 cm spacing. The resulting dataset and logarithmic model shown is in Figure 3.

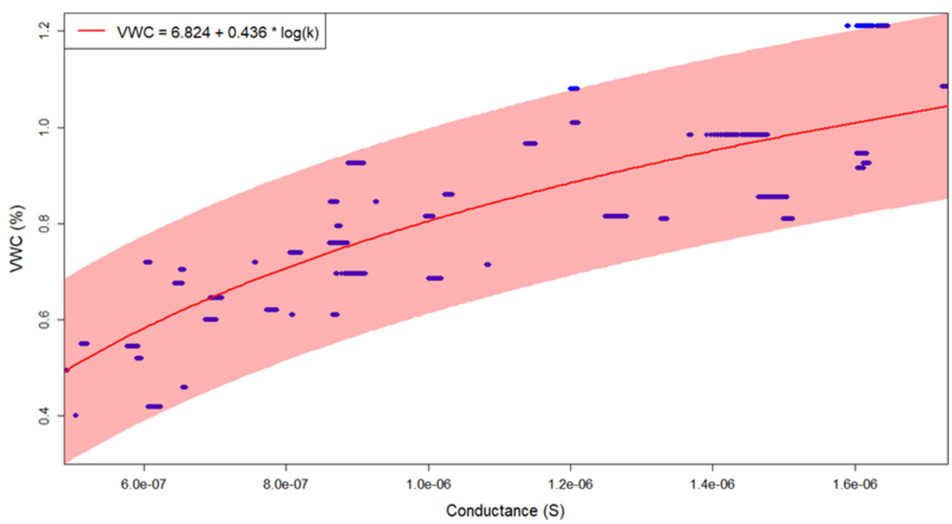

FIGURE 3 | Logarithmic model with 95% prediction interval for VWC (%) versus conductance (S) for Wetterstein Limestone.

After each experiment, the two 16,000 cm^3 rock samples were fully saturated by immersion and electrical conductance data for each depth interval collected. The values from this are then used to adjust the estimated volumetric moisture content VWC (%) data from the experiments to relative pore saturation (%) as spatial heterogeneity of porosity in the samples (Figure 1b) means comparison by VWC could potentially be misleading.

2.5 | Moisture Movement Process Periodisation

A periodisation of the moisture data was created to identify distinct moisture movement processes over time. To achieve this, the moisture saturation data for each depth was smoothed using a centred moving average with a 100-min window. Local trends in moisture dynamics were quantified by applying a rolling linear regression over an 80-min window. Trend classification was then applied to the resulting slope values, identifying periods of increasing (> threshold), decreasing (< −threshold) or stable (≤ threshold) moisture dynamics. Changepoints in these trend patterns were detected using the PELT (pruned exact linear time) method [46], with a fixed penalty value of 0.005 to control detection sensitivity.

To further define different moisture movement processes, the rock moisture phase was defined. The formation of frozen, solid phase rock moisture was defined by either a sudden drop in rock moisture (as seen in soil freezing characteristic curve (SFCC), [47]) and, when present, latent heat isotherms. The resulting temperature ranges can be seen in Figure S1. In the case of spontaneous freezing of rock moisture that is supercooled, there is a marked moisture drop due to the rapid phase change and generally is accompanied by a latent heat fusion spike, the size of which is related to the degree of supercooling [48]. Meanwhile, more gradual freezing events are often not easily discernible in the moisture data and better defined by temperature data. The freezing points identified by some of the moisture data can be seen to be above 0°C. This is probably for several reasons. Firstly, the temperature sensors themselves were not at the exact location of the electrode pairs and so the 1D temperature data model may not be completely accurate for that point. Secondly, the temperature sensors are affected by both the rock and rock moisture temperature. It is possible that the rock moisture in the fractures was in fact already below freezing, due to nonconductive heat transport caused by rock moisture movement [49] and so could begin to freeze despite the surrounding rock temperature being above 0°C. Over experimental time, freezing points showed a decrease in temperature, probably due to the effects of dissolution on rock moisture chemistry [50]. The rock moisture was defined as in a thawed liquid phase when the temperature at that depth rose above 0°C again.

The results from one exemplary periodised freeze–thaw cycle incorporating the frozen/unfrozen rock moisture state and moisture movement trend are shown in Figure 4a,b and defined below:

> Thawed: rock moisture in the unfrozen state. Capillary rise is defined by moisture increasing towards the surface of the sample. Gravitational moisture movement is defined by moisture increases towards the base of the sample.
>
> Freezing: rock moisture > 4 cm depth from surface is in unfrozen state, but surface rock temperatures are ≤ 0°C. Moisture movement seen towards the surface, governed by cryosuction (cryo to surface, Figure 4b).
>
> Frozen: rock moisture in frozen state. Frozen decrease (grey, Figure 4b) is defined by the slow decrease in rock moisture as the remaining liquid phase water gradually freezes in turn creating pressure at fracture tips through VE. There is also a frozen increase (dark blue) of rock moisture from the base seen in this period. This is interpreted as being evidence of IS.
>
> Thawing: when the air temperatures increase and begin to thaw the rock surface (> 0 °C) and progressively at greater depth in the sample. The dominant moisture movement process in this time is cryosuction towards the base or frozen zone (cryo to base, Figure 4b).

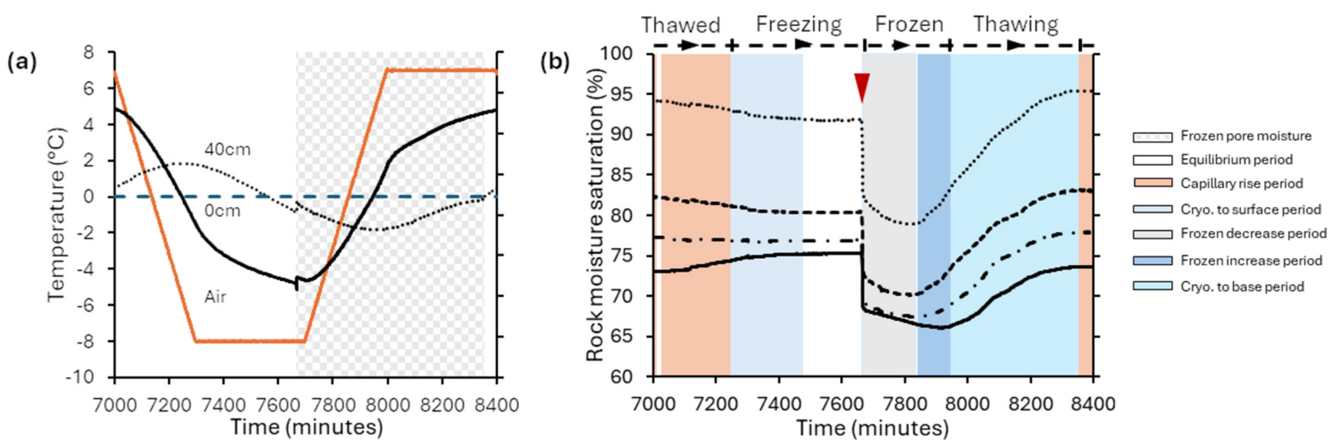

FIGURE 4 | Periodisation of temperature and moisture cycle. Data displayed from an exemplary diurnal cycle in exp.75+. (a) Temperature cycle with air and rock temperature, periods with frozen rock moisture (grey). (b) Average rock moisture for different depth intervals in samples, with different moisture movement processes. The point of spontaneous freezing in this example is marked by the red arrow.

During any period, there can be times of equilibrium (white, Figure 4b) where the rock moisture levels stay apparently constant at a given depth but could also be the result of even displacement and replacement of rock moisture.

2.6 | Acoustic Emissions

2.6.1 | Filtering

The recorded AE hit data were analysed with AEwin for the Micro-SHM V1.50 software from MISTRAS Group Inc. The data were filtered with peak and average frequency range of < 10 and > 120 kHz being rejected due to the resonate frequency (60 Hz) of the AE sensors. To further filter for background noise, AE signals with absolute energy < 5 aJ were rejected [11].

2.6.2 | Location Procedure

For locating the AE signal distance from sample surface, a linear location mode in the Micro-SHM software was used. This needs at least two AE hits to create an AE event. This method counts the delay in arrival time between the two AE hits and calculates the source location by linear interpolation between the two AE sensors to give a depth from surface [51]. Due to location uncertainties caused by the heterogeneity of the rock samples, largely fracture-based porosity [52], the data were then subsequently zoned into AE events occurring between 0 cm < 10 cm, 10 cm < 20 cm and 20 cm < 30 cm from sample surface. During the experiment, hourly average signal time (AST) pulses between the acoustic sensors checked for changing wave speed between the sensors. Based on this, wave velocity was set individually for each sample and experiment run. Furthermore, due to the significant change seen in velocity as a result of rock moisture phase change, different velocities were used during frozen and unfrozen periods (S7).

3 | Results

3.1 | Rock Moisture Movement

3.1.1 | Moisture Saturation Over Cycles

Across the whole experiment, all runs showed an increase in overall rock moisture (see Figure 5). This is thought to be because during experiment preparation and 24 h cooling time for the samples, a gravitational effect meant that previously evenly distributed rock moisture concentrated at the base of the samples (evident in starting saturation distribution of all samples in Figure 5) and pooled at the clingfilm sealed base. As our rock samples are low porosity (ca. 0.7%), only a small amount is needed to be a considerable water source for the

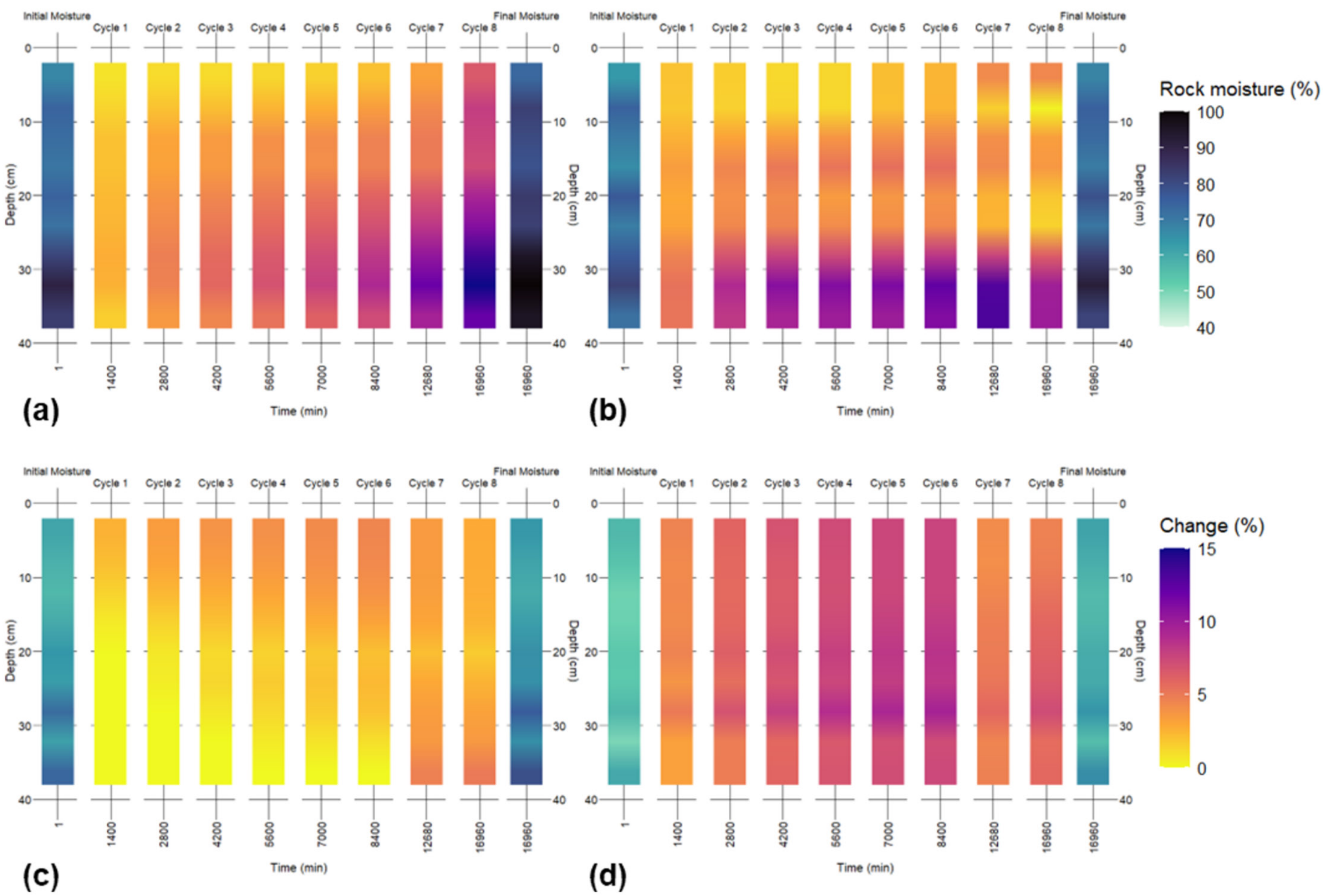

FIGURE 5 | Initial and final rock moisture saturation (%) at depth in each experiment run (a) exp.75+, (b) exp.70, (c) exp.60 and (d) exp.50. Percentage rock moisture change from starting saturation after each F/T temperature cycle.

experiment. The rock moisture increase seen is in the range 3.0% to 15.0%, with sample exp.75+ run having the greatest increase. The exp.75+ sample also shows moisture saturations of over 100% near the base. This is probably due to the extra pressure from freeze–thaw processes causing increased saturation in pores not accessible by the original sample saturation method of immersion (which the saturation calibration was based on).

Throughout the cycles, the rock moisture increase does not occur evenly across the experiment. In the first shorter 1400 min freeze–thaw cycle, all experiment runs apart from exp.60 see an overall moisture increase of ca. 2% to 4%. In the remaining five shorter freeze–thaw cycles, all experiment runs see an increase in rock moisture of ca. 0.5% to 1.5% per cycle. However, during the longer cycles, only the exp.75+ run maintains a similar rate of increase. This is suggested to be evidence of more external rock moisture being available at the base of the sample than in the other experiment runs.

3.1.2 | Moisture Movement Processes

The results of periodised moisture movement processes are shown below:

3.1.2.1 | Thawed. Evidence of capillary rise can be seen in all experiment runs in Figure 6a with a notable increase in rock moisture towards the surface. The capillary rise effect is enhanced when there is a temperature gradient in the rock causing a capillary pull to the cooler surface area due to the creation of a vapor pressure gradient and increased further by the presence of ice [53]. All experiments show a similar change.

3.1.2.2 | Freezing. In Figure 6b, exp.75+ and exp.70 show a similar rock moisture increase at surface with the exp.75+ showing the greatest increase of the two experiments. The exp.60 and exp.50 show more total moisture increase and to a greater depth; however, in these experiments, spent more time in an unfrozen state (Figure 7), so consequently longer with conditions allowing cryosuction to surface in the freeze–thaw cycles. During this time, the rock moisture can be seen to reach supercooled temperatures in most cycles (not shown) before the onset of spontaneous freezing (an example of this shown by the red triangle in Figure 4).

3.1.2.3 | Frozen. The period after this is defined by a slow decrease in rock moisture as the remaining liquid phase water gradually freezes (frozen decrease in Figure 4). As would be expected, this is most pronounced in the exp.75+ experiment (Figure 6c) due to more rock moisture being available to change state. After this period of decreasing liquid rock moisture, we start to see an increase in rock moisture from the base of the samples while there is still frozen rock moisture present (frozen increase in Figure 4b). This increase of rock moisture from the base is interpreted as being due to cryosuction of remaining rock moisture trapped at the base of the samples, consequently promoting IS and associated crystallisation pressures [54]. The greatest increase is unsurprisingly seen in exp.75+ (Figure 6d), which had the greatest availability

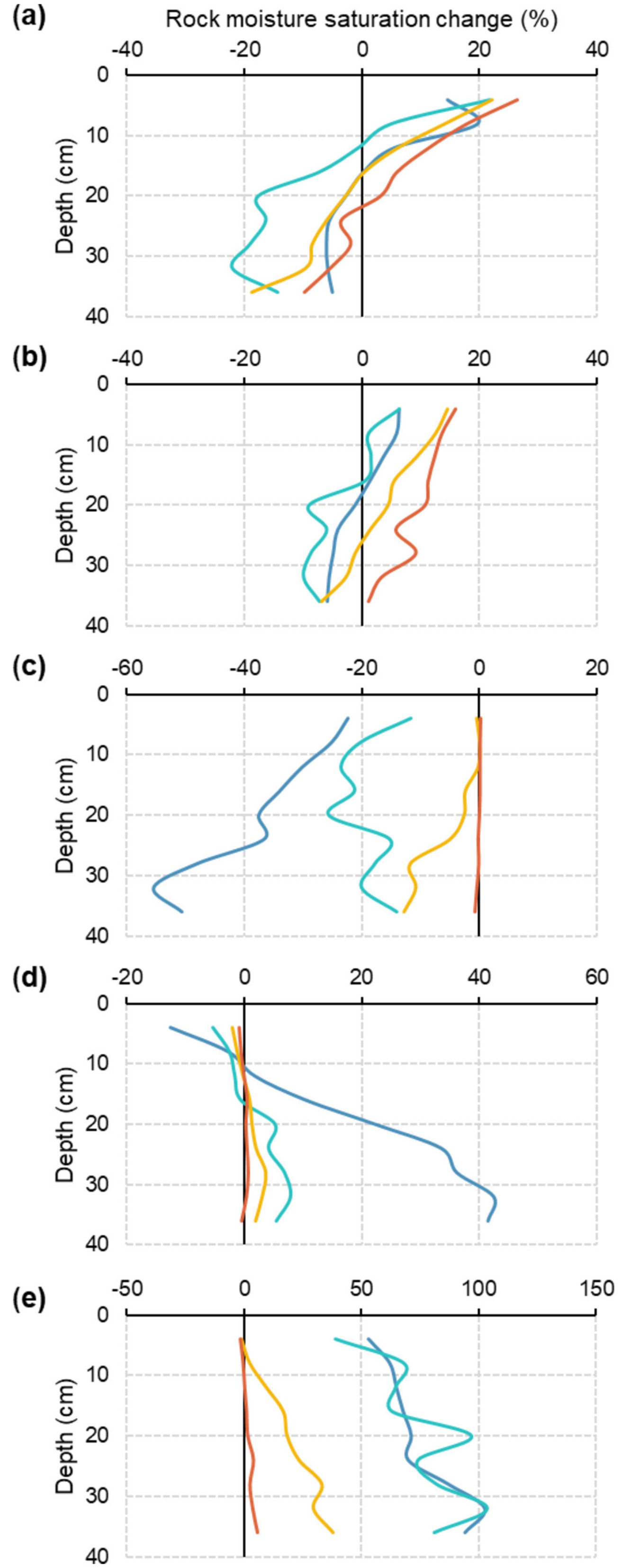

FIGURE 6 | Total rock moisture saturation change at depth from surface over different moisture movement periods assigned in Figure 4. exp.50 orange, exp. 60 yellow, exp. 70 turquoise and exp. 75 blue (in supporting information S2–S6, bar plots are stacked showing diurnal (blue) and ca.72 h (orange) cycles total moisture change at depth from surface).

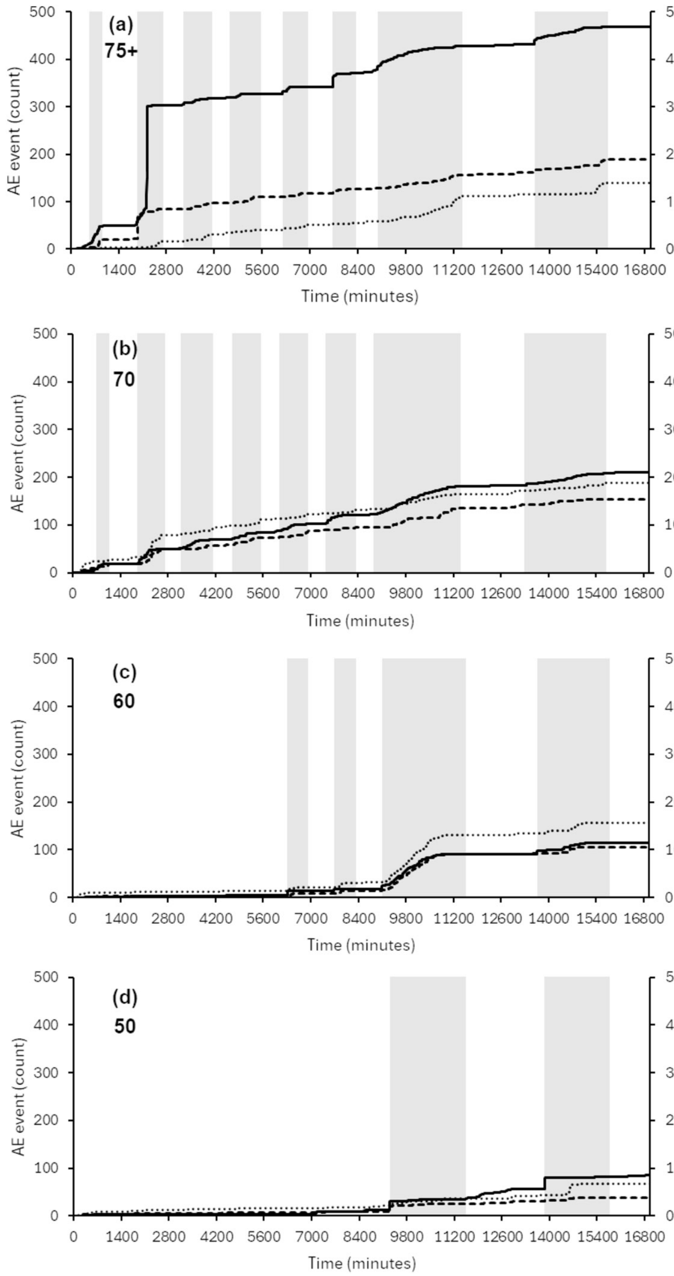

Depth	Diurnal	72 hr
0-10cm	371	98
10-20cm	127	62
20-30cm	55	85
Total	553	245

Depth	Diurnal	72 hr
0-10cm	120	91
10-20cm	95	59
20-30cm	132	56
Total	347	206

Depth	Diurnal	72 hr
0-10cm	18	97
10-20cm	14	92
20-30cm	31	128
Total	63	317

Depth	Diurnal	72 hr
0-10cm	8	77
10-20cm	8	31
20-30cm	18	50
Total	34	158

FIGURE 7 | Cumulative AE Event count for experiment runs exp.75+ (a), exp.70 (b), exp.60 (c) and exp.50 (d). Solid line 0–10 cm depth from surface, dashed line 10–20 cm depth and dotted line 20–30 cm depth. Tables show the totals for cycles over the 6 ca. diurnal F/T cycles (8400 min) and following ca. 72-h F/T cycles. Grey shaded areas show the time periods when there is rock moisture present in a frozen state through the entire sample.

of moisture at the base. exp.50 shows little to no decrease or increase in apparent rock moisture during the frozen phase. This is probably a combination of being lower in rock moisture saturation and being on the edge of the instrument's detection range.

3.1.2.4 | Thawing. When the air temperatures increase and begin to thaw the rock surface (> 0 °C), instead of seeing an initial increase in rock moisture, we actually see a decrease at surface (not shown) due to the newly available rock moisture being pulled by cryosuction towards the progressively retreating frozen front. After a while, the frozen zone of the rock can no longer accommodate more rock moisture and an increase at depth seen in Figure 6e is related to the phase change back to higher conductivity liquid state rock moisture.

The sample with lowest overall saturation (exp.50) shows a very limited increase during Cryo to base movement. This is probably due to it having the biggest moisture data gaps from being on the edge of the instrument's detection range at these temperature and moisture conditions.

Through all phases of the freezing cycle, Figures S2 to S6 show that the shorter diurnal cycles cause greater moisture movement than the longer ca. 72-h cycles, over a similar total time period.

3.2 | Rock Weathering

3.2.1 | AE Events Over Time

The amount of rock moisture in the samples is also seen to affect the duration of the frozen phase rock moisture. To determine when rock moisture is frozen, first, a rapid decrease relative to the initial rock moisture content was identified. The equivalent depth is considered thawed when temperatures over 0°C are reached. The results of this periodisation can be seen in the grey shaded areas of Figure 7, with experiment runs with greater starting rock moisture (exp.75+ and exp.70; Figure 7a,b, respectively) showing evidence of frozen rock moisture from the first and second freeze–thaw cycles respectively. Meanwhile, rock moisture in the lower saturation exp.60 (Figure 7c) only freezes by Cycle 5 and in exp.50 (Figure 7d) only by the longer freeze–thaw Cycles 7 and 8. This difference in time in the frozen state affects which rock moisture movement processes are prevalent in the samples. The decrease in rock moisture caused by phase change to ice combined with the low conductivity of the Wetterstein limestone samples and decreasing temperatures meant that there are unfortunately some rock moisture data gaps where the conductivity consequently became too low for our instrument. In the lower starting saturation experiment, the rock moisture was most likely present in the smaller pore spaces in the rock, as the larger more permeable areas of the porosity would be the first to dry when getting the sample to starting weight. In smaller pores, the rock moisture has a depressed freezing point and so needs more time at lower temperatures in order to freeze.

The results show most AE events overall with the highest saturation experiment with 798, 557, 380 and 192 AE events in total for exp.75+, exp.60, exp.60 and exp.50 respectively. Over the six diurnal cycles, there are 1.7× to 2.3× as many AE events in the two more saturated samples (exp.70 and 75+ respectively) as in the two following 72-h cycles. However, the two lower saturated samples see very few AE events in the diurnal cycles, with a 4.6× to 5× increased rate of AE events in the 72-h cycles. This shows the importance of rock moisture changing state and the related processes involved to rock weathering as these two samples are only in a frozen state in the later temperature cycles. In all experiment runs, the highest rate of AE events can clearly be associated with freezing events during the temperature cycles. Interestingly, the exp.60 and exp.75+ show the greatest count of AE events in the 72-h cycles. One reason for this could be the continued availability of water from the base of the sample (see Figure 5) for promoting IS unlike the other experiment runs, which show a decreased availability of rock moisture from the base of the sample during Cycles 7 and 8.

The totals of AE events in the different depth zones show different distributions relative to the two different sample blocks used. This is probably due to differences in the pore space distribution within the samples derived from the saturated electrical conductance distribution seen in Figure 1b, showing higher values at the base of the sample, suggesting greater effective porosity and in turn more fractures to propagate during weathering cycles.

There is some effect of cyclicity seen during the temperature cycles, with each experiment having more prominent zones of maximal AE event rate, which are not matched again through the rest of the experiment (for example diurnal cycle 2 in exp.75+). This is probably due to the Kaiser effect [55] and the heterogeneous distribution of the porosity within the rock samples leading to areas of localised stress concentrations, thereby increasing the likelihood of seemingly random spikes in AE event activity.

3.2.2 | AE Events by Rock Moisture

From the overall AE event count for each experiment run shown in Figure 7, higher overall rock moisture saturation relates to more overall AE events. When the average rock moisture from the different depth zones at the beginning of a freezing cycle and the subsequent AE events that occurred until reaching a thawed state is taken into account, as in Figure 8, it can be seen that rather than linearly increasing with increased rock moisture, there is in fact a peak AE intensity period in the range from 65% to 75% moisture saturation. This range of starting rock moistures accounts for 62.1% of all recorded AE events. An initial average moisture saturation of $< 55\%$ and $> 85\%$ was not recorded in depth zones with AE sensors in our experiment; however, greater saturation was seen at the base of the sample at 30 to 40 cm from the surface.

3.2.3 | AE Events During Freezing Cycle Periods

By breaking the freezing process down into different periods of thawed, freezing, frozen and thawing, we see that by far the greatest amounts of AE events were recorded in the frozen period of all experiments at 63% (Figure 9d), with increasing saturation showing more total AE events. This trend is also evident in the freezing and thawing periods, but at 14% to 15% respectively of the overall AE event count. In general, the opposite is true for the AE event count in the thawed periods with the

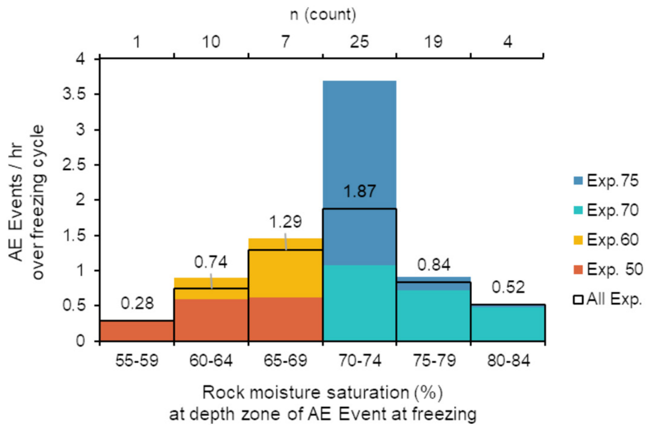

FIGURE 8 | AE events/hour for freezing cycles, categorised by rock moisture saturation at the start of a freezing cycle at different depth zones. These depth zones are pooled together and resulting rates for different experiment runs (exp.50 orange, exp.60 yellow, exp.70 turquoise, exp.75+ blue) and overall (black line and labels) are shown. n = the number of freezing cycles in the corresponding starting moisture range.

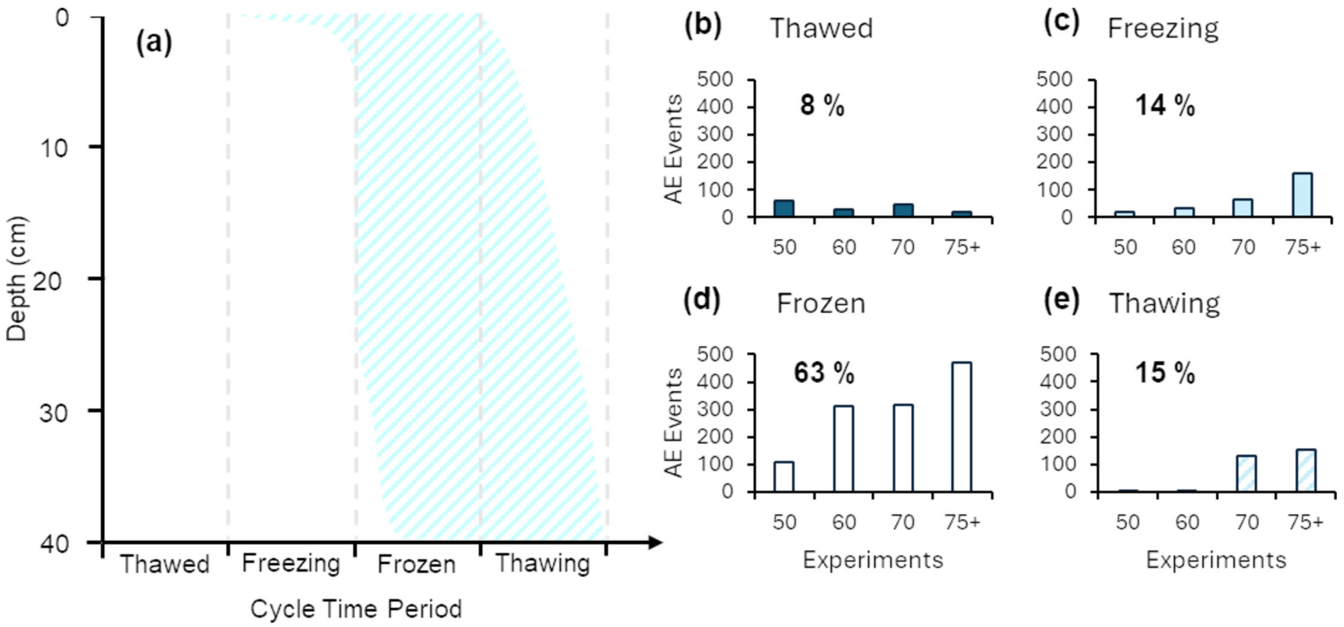

FIGURE 9 | (a) Schematic diagram showing different periods of freezing cycle seen in the experiment (blue hatching = occurrence of frozen pore water); (b) AE event count for the different experiments when rock moisture is Thawed; (c) AE event count for the different experiments when rock moisture is Freezing; (d) AE event count for the different experiments when rock moisture is Frozen; (e) AE event count for the different experiments when rock moisture is thawing.

lowest saturated exp.50 showing the highest AE event count, however on a much lower absolute level.

3.2.4 | AE Events at Depth During Freezing Cycle Periods

In Figure 10a, the most AE events are seen by the frozen fringe at the surface of the sample. This is probably due to a combination of thermal stresses and increased hydrostatic pressure from cryosuction to the frozen front at the rock surface. In addition to this, there is probable frost wedging in the larger pore spaces at the surface.

During the frozen period, there are three to five times as many AE events at any depth. At the start of a cycle, when the rock moisture is steadily decreasing, due to rock moisture changing phase to ice, VE is the dominant factor. Figure 10b(i) shows that the greatest AE event count is in the 0–10-cm zone. This is probably due to it being in this period for longest and experiencing greatest thermal stress. For the data in this study, IS is defined as periods where there is frozen rock moisture and either an increase in rock moisture recorded or an equilibrium. In addition, there are periods at the lowest temperatures and liquid rock moisture content where there is no moisture data. Due to these periods being in the frost cracking window (Fcw) of −3°C to −8°C [56], IS is assumed to be the dominant stressing process.

As the block thaws and more liquid water becomes available at the frozen fringe, a marked increase in AE events can be seen in this area (Figure 10c). Throughout the thawing period, but particularly from (iii) on (where more liquid rock moisture becomes available), the maximum AE event intensity with depth closely follows the retreating frozen fringe as the sample thaws. This shows that the area by the frozen fringe is a zone of high rock weathering, which is increased with increased rock moisture availability.

3.2.5 | Moisture Movement Processes and AE Events

3.2.5.1 | Diurnal Cycles. When comparing AE event intensity by rock moisture movement process time, VE shows the greatest cracking intensity, on average, as a process in diurnal cycles and also in longer 72 h cycles, though to a lesser degree (Figure 11a,c). The mean rate is notably skewed from the median in the diurnal cycles due to the particularly high AE rates seen in exp.75+ compared with the other experiment runs (see Figure 7). IS has the next highest AE event rate, followed by cryo to base during thawing.

3.2.5.2 | 72-h Cycles. In the longer 72-h cycles, VE remains the process with greatest weathering intensity. However, IS shows greater significance over full cycle time with the mean AE rate more than doubled. This will be because crack propagation from VE happens in more sudden bursts while the pressure buildup from IS is more gradual.

The processes seen during the thawed periods (capillary rise, gravitational, equilibrium) all have slightly decreased weathering significance in the 72-h cycles, likely because of less cyclic thermal stress than in the diurnal cycles.

3.2.5.3 | Across All Cycles. When considered over the total experiment time (Figure 11e), IS is seen to be of greatest importance to rock weathering in freeze–thaw cycles.

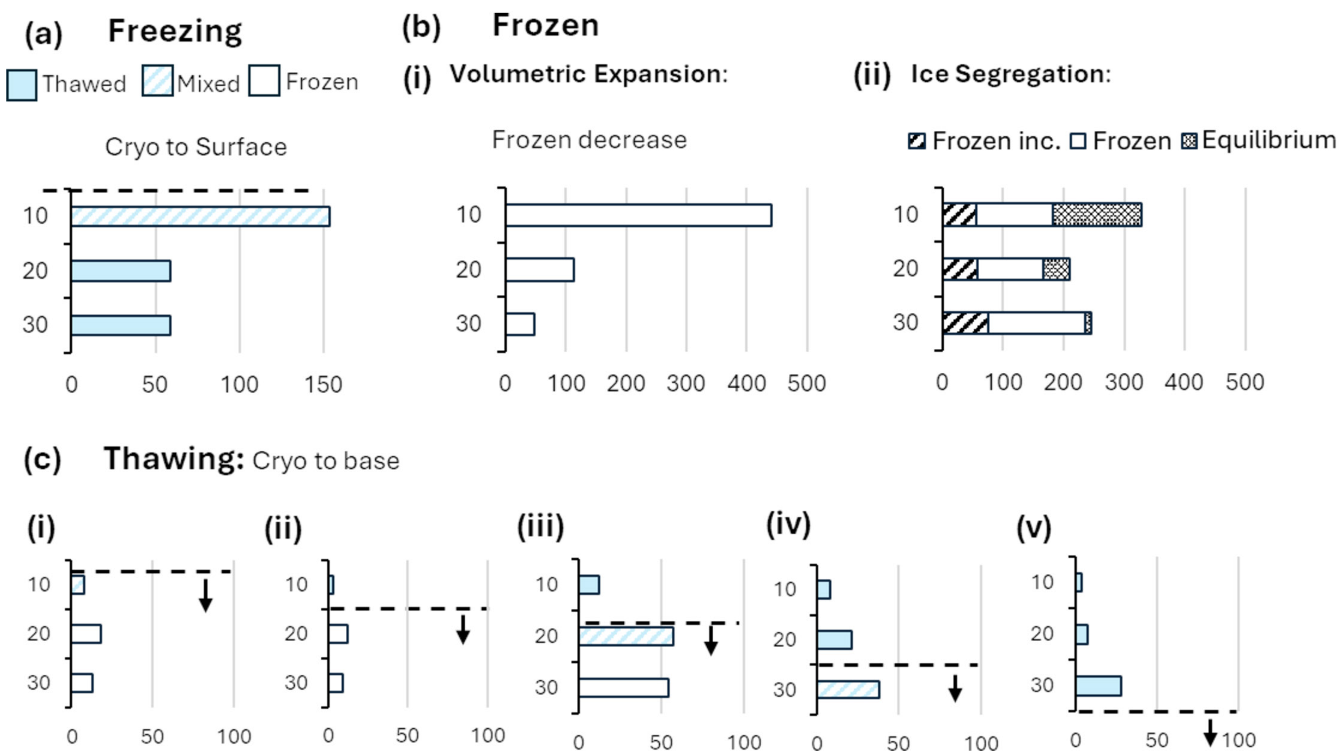

FIGURE 10 | AE event count across all experiment runs at depth 10 (0–10 cm), 20 (10–20 cm) and 30 (20–30 cm), from sample surface. (a) Freezing period—when cryosuction to the surface is seen (Figure 4a). (b) Frozen period—(i) volumetric expansion (decreasing rock moisture during continued freezing—frozen decrease) (Figure 4b) and (ii) ice segregation. (c) Thawing period—with cryo to base (Figure 4c) moisture movement (i–v). Dashed lines show location of the frozen/unfrozen boundary, and arrows show direction of movement during that time window.

Cryosuction to the base during the thawing period is also very important to rock weathering, particularly with increased rock moisture availability (increasing the range of AE rates seen). Increased thermal stresses from more temperature cycles and repetition of the frozen/unfrozen interface traveling through the rock sample probably account for the increase in AE rate from 0.2/h in the 72-h cycles to 0.3/h mean rate in the diurnal cycles. Capillary rise and cryosuction to surface both show similar AE rates over the total experiment time, with both showing more significance during diurnal cycles.

Overall, the relative rock weathering effect of different processes over total experiment time, based on median AE event intensity is:

Ice Segregation > Volumetric Expansion > Thawing (Cryo to base) > Cryo to surf/Capillary rise > Gravitational > Equilibrium.

3.2.6 | Ice Segregation Efficacy Temperature Range

By looking at the AE events rate per hour by temperature during IS, Figure 12 shows the process starts to cause crack propagation from −1°C, while the maximum rate can be seen from −4°C to −7°C. This would suggest a Fcw in this range for Wetterstein limestone. A limitation of our experiment is that rock temperatures did not fall below −8°C or remain at that level for extended periods, so stronger weathering effects may occur at lower temperatures.

4 | Discussion

4.1 | Limitations of Study

There is an attenuation of AE signals over distance [57]. This means that many apparently lower amplitude, yet important AE signals may have been missed due to falling below the 30-dB threshold. The resulting characteristics of the detected signals may also give a false impression particularly when performing AFRA analysis to determine whether AE signals are from tensile, shear or mixed-mode cracking. Furthermore, the important aspects of wetting and drying on physical rock weathering [58, 11] at the rock surface and the additional AEs produced by fracture propagation are probably largely undetected with this experimental setup. Future work ensuring an AE sensor is present directly on the sample 'surface' would ensure that this weathering effect is not missed.

Additionally, more sensors, probably a minimum of 8 in total, would be best to ensure that distance between sensors is reduced and that moment tensor analysis could be used to increase the accuracy of AE signal location and adjust the characteristics of the recorded waves based on distance and velocities of the materials. This would also have the benefit of being able to apply and compare the results of models developed by Maji and Murton [40] on rock weathering. Also, due to the heterogeneity of the porosity in Wetterstein limestone, it is suggested that μCT scanning is used to better determine the pore structure [42, 59, 60]

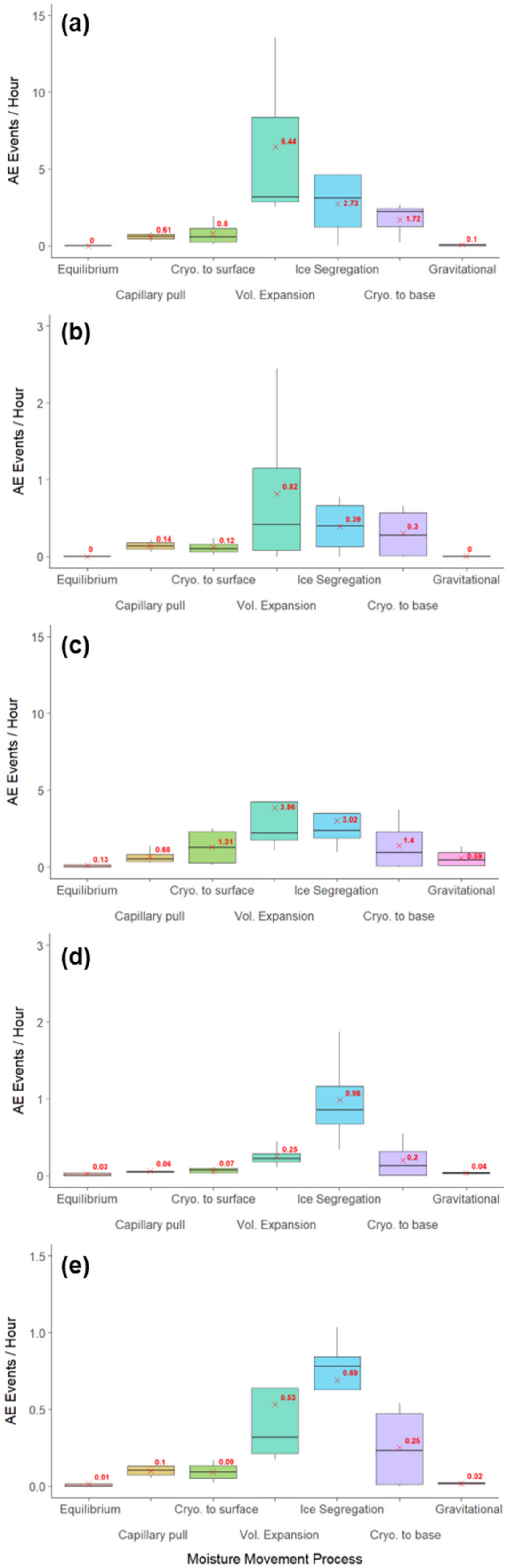

FIGURE 11 | The AE event rate per hour by rock moisture movement process across diurnal cycles (a) by process time (= intensity) and (b) by cycle time (= significance to cycle length). The longer 72 h cycles are shown in (c) by process time and (d) by total experiment time. All processes considered over total experiment time (= overall significance) are shown in (e).

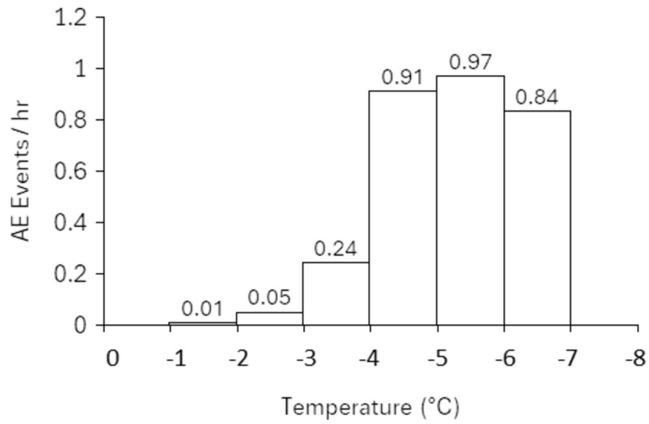

FIGURE 12 | Histogram of the AE events/hour by average temperature recorded in depth zones when AE events were recorded, during periods of ice segregation.

and its effect on signal attenuation when locating fracture propagation source.

In the moisture data, there are unfortunately some gaps at the coldest temperatures where the combination of electrical conductivity's temperature dependence and low unfrozen rock moisture content means it is out of the instrument measurable range. This range could be tailored to the lower conductivity ranges of our rock samples with the addition of a different pre-resistor. The number of rock samples and temperature cycles are also a potential limiting factor in the study. As only two rock samples of low-porosity Wetterstein limestone were used in the study, it may be that the randomness of pore structure in the individual samples has impacted the experimental results, requiring further repetitions in future projects. In addition, there could be a preconditioning bias of the diurnal freeze–thaw cycles caused by the temperature cycle setup always starting with these ahead of the 72-h cycles [61], so the weathering effect of starting with longer temperature cycles should be conducted in future experiments.

Finally, our study focussed on one lithology type, Wetterstein limestone. While the results should be comparable in lithologies of similar tensile strength and fracture based, low effective porosities (< 5%), differences in grain size in granites [26], rock chemistry [62] and foliation in gneiss [63] could affect the weathering outcome. In an experimental study by Duca et al. [27] of an intact, low-porosity Arolla gneiss, greater frost cracking weathering occurred in warmer temperatures (−0.5°C to −2.7°C) than our Wetterstein limestone samples (−4°C to −9°C), suggesting a comparably higher weathering rate than seen in our study.

The behaviour of higher porosity (> 20%) sandstone rockwalls meanwhile would undoubtedly be quite different, with vastly different porosity structure, permeability and tensile strength. A study by Maji and Murton [64] shows macrocracking occurring in chalks after eight freeze–thaw cycles and 16 cycles in sandstones, something which did not happen with our samples. This could be due to frost weathering already occurring at warmer temperatures in such rockwalls [28].

4.2 | The Effect of Rock Moisture Saturation and Time on Rock Weathering

Our results suggest that higher overall rock moisture saturation leads to greater AE event count (see Figure 7) and so an increase in rock weathering over the course of repeated freeze–thaw cycles. However, when AEs are considered by unfrozen rock moisture saturation at depth (Figure 8), an apparent peak AE intensity is seen between 65% and 75%, with lower and higher saturation showing decreased evidence of fracture propagation. This would be in line with suggested lower saturation thresholds for IS of 58%–65% [65, 66, 67], derived from studies on limestone, tuffs and chalk respectively. An earlier study by Mitchell and Sass [11] also found that Wetterstein limestone rock samples with 50% and 100% moisture saturation had very similar overall AE counts, with the 50% run even having a slightly greater count, suggesting increased moisture saturation eventually becomes a limiting factor in physical rock weathering. This is probably due to the changing properties in rock strength and plasticity caused by increasing rock moisture [68]. Furthermore, while a higher starting saturation (> 91%) at the freezing point may cause greater initial crack propagation through VE [28, 69], it will also promote a rapid reduction in hydraulic conductivity within fracture-controlled porosity as ice formation constricts fracture apertures and limits flow to thin pre-melted films [70, 71]. This transition markedly decreases the rate of pore-water migration through the frozen zone [71], and because sustained moisture availability is a prerequisite for IS and segregation-driven crack propagation [67], elevated initial saturation may ultimately inhibit long-term fracture growth relative to the peak weathering saturation range of 70%–75% observed in our experiments.

Rock weathering was also seen to be affected by the rock moisture saturation and the duration of freeze–thaw cycles. Mayer et al. [42] observed that, over a given time period, a greater number of shorter freeze–thaw cycles cause more fracturing than fewer, longer cycles due to increased thermal stressing; however, this effect is found to be dependent on rock moisture saturation in our experiment. In the more saturated exp.75+ and exp.70, rock moisture became frozen in all diurnal and 72-h cycles. In the lower saturated experiments, however, rock moisture was only frozen in the later diurnal or even only in the 72-h cycles, due to a depressed freezing point compared with the more saturated runs (S1). This leads to a decreased weathering effect as the higher efficacy processes associated with frozen rock moisture do not occur. The reason for the depressed freezing period in lower saturation samples is that bulk water in larger interconnected pores evaporates preferentially to rock moisture in smaller pores [72]. This leaves a higher ratio of rock moisture in smaller, more disconnected pores in lower saturated areas, thus depressing the freezing point due to the Gibbs–Thompson effect [73] and decreasing the thermal conductivity relative to more saturated areas [74, 75]. The result also shows that, in our experiment, the weathering efficacy of thermal stress alone in freeze–thaw cycles is lower than that of a rockwall with sufficient freezing time and moisture availability.

4.3 | The Effect of Moisture Availability and Movement on Rock Weathering

While saturation is shown to affect rock weathering efficacy and timing [11], from the results of single long freezing cycles conducted by Mayer et al. [10] on Wetterstein limestone, it was shown that initial moisture saturation was less important than rock moisture availability. Therefore, during any rock moisture limited processes, the rock permeability determines the ultimate availability of rock moisture from different areas of the rockwall [49].

Thermodynamic processes lead to rock moisture movement through capillary pull forces: capillary rise, gravitational, wetting and drying, which have all been shown to affect rock weathering [11, 76]. When pore water freezes, the short-lived pressures from VE [77] are affected by saturation and pore geometry [78]. The increased efficacy seen in this study during periods of IS (Figure 12) requires the availability of more rock moisture drawn to the ice lens by cryosuction (Murton et al. [67]; Walder and Hallet [69]). A low permeability would limit this process [79, 80] and so the potential overall weathering effect of a freeze–thaw cycle, even in the case of higher initial rock moisture saturation.

Evidence from our results for the increased effect of water availability on rock weathering can particularly be seen in the longer 72-h cycles of exp.70, exp.60 and exp.50. In all cases, a decrease in rock moisture relative to the start of a freeze–thaw cycle (see Figure 5) shows a decrease in AE count relative to cycles with more moisture availability (see Figure 7). Further evidence of the importance of moisture availability is seen during the top-down thawing of the experiments. As the frozen fringe retreats, the AE intensity becomes greater with increased depth from the surface due to increased moisture availability for IS. This confirms the results of other research [12] showing that in locations with permafrost, the frozen fringe is likely to be the area of greatest fracture propagation.

4.4 | Frost Cracking Window Temperature Dependence

As IS was confirmed as the process of greatest rock weathering efficacy in freeze–thaw and sustained freezing cycles, the Fcw [56] is useful to define for analysing field data. Walder and Hallet [69] suggest frost cracking occurs in a range of −4°C to −15°C and varies with rock strength [81], with some studies showing frost cracking still occurring in temperature ranges up to −1°C [82], thus making the application of a general Fcw across different lithologies unreliable [10].

Our results confirm that in Wetterstein limestone, the IS appears to begin from as soon as −1°C (in line with field studies by [82]) with sharply increased efficacy by a factor of 10 from −4°C until −7°C (Figure 12). This would suggest a Fcw of −4°C to −7°C. However, due to the limited temperature window of our experiment going down to a minimum temperature of −8°C in the near surface, we cannot confirm the suggestion of Mayer et al. [10] that the greatest efficacy in frost cracking is seen from −7°C to −9°C in the same lithology. A limitation of their study is that the lowest temperatures were reached in a rapid, continuous drop from ca. 10°C to −10°C followed by a gradual, stepped thawing, which could bias microcracking to colder temperatures. An interesting continuation to this study would be to see if maximum weathering efficacy is still seen at these lower temperatures with a more gradual stepped cooling. Due to the higher viscosity of water at temperatures below −9°C, the migration of water is inhibited [83] and so likely inhibits the weathering efficacy of IS at lower temperatures. For now, we would recommend an expanded Fcw of −4°C to −9°C for Wetterstein limestone.

4.5 | Implications for Wetterstein Limestone Alpine Rockwalls

Results showed that while capillary rise and gravitational moisture movement processes do cause physical weathering (Figures 9 and 11), the freezing of rock moisture and the associated processes are far more effective physical weathering agents. Ice formation also creates zones of increased hydrostatic pressure both from top-down and bottom-up moisture supply [13, 12]. The retreat of the frozen fringe during our experiment—analogous to retreating permafrost—displays a high level of rock degradation following the frozen fringe (Figure 10). Analysis of AE rates per hour showed that VE is generally creating the highest AE intensity over processes specific time, particularly over shorter diurnal cycles (Figure 11a). However, when considered over total freeze–thaw cycles time, IS has a much greater AE intensity (Figure 11e), implying greater subcritical crack propagation/widening efficacy, particularly in longer cycles (Figure 11d). This shows that while VE is the most destructive individual process, when considered over complete cycle time, the more gradual process of IS has greater geomorphic effectivity [84].

While in our experiments there was only a limited amount of moisture availability outside of the frozen zone, it may be that in calcareous alpine rockwalls, even more rock moisture is available at depth. Rode et al. [2] suggest > 60% rock moisture saturation, and Sass [13] states that > 70% is available at depths > 20 cm, so a more common natural comparison would be to our exp.75+ where there was greater rock moisture available throughout the cycles. The other experiment runs are more applicable to rockwall zones with permeability such as detached blocks, porosity heterogeneity or fault gouge [85, 86, 87].

Climatic conditions in calcareous alpine rockwalls are shown to vary with aspect and elevation, with varying moisture availability and recharge affected by inclination [2]. Our identified moisture movement periods and their relative weathering efficacy would suggest that greater efficacy of physical rock weathering is seen during freeze–thaw cycles at rockwalls with a northerly aspect (in agreement with [30, 88]), due to their longer, colder cycles and moisture availability at depth to create favourable conditions for IS [80]. Southern facing rockwalls areas near to a snowfield but exposed to the increased temperature fluctuations seen on south faces would likely have an increased rock moisture supply and so potentially have similar weathering efficacy to the longer cycles seen in Northern facing rockwalls, especially considering the increased thermal-stress-related cracking seen with the higher magnitude temperature fluctuations [38]. In addition, the summed effect of more wet/dry cycles and hydrostatic pressures from capillary moisture fluctuations may end up reducing the aspect-dependent difference in overall rock weathering. Finally, the lower Fcw temperature range than stated in Rode et al. [2] would suggest a greater time in conditions favourable for IS and so greater physical weathering in colder northern aspects at higher altitude. However, with the warming climate, other rock moisture processes may start to play an increasingly important role in the degradation of alpine rockwalls. Future development of a thermo-hygromechanical model to test these findings on field data is needed to understand the full effect of this.

5 | Conclusions

Our experimental findings highlight the role of rock moisture, its movement under freeze–thaw cycles and its effect on physical rock weathering. The occurrence of more AEs with greater overall moisture saturation suggests increased moisture is beneficial to weathering efficacy. However, our results also show that the peak of cracking intensity occurs at saturation levels of 70%–75%, which means that even higher saturation is not required. This suggests that there is a self-limiting effect, probably due to changing rock fracture mechanical properties and to a decreasing ability of water to move within the pore space. This means that assumed preconditions for effective frost weathering (e.g. required saturation of > 91%) must be questioned. Length of freezing cycle in interplay with saturation also plays an important role in weathering effect. This is due to the rock moisture in lower saturated areas of rockwall being preferentially contained in smaller pore diameters, leading to a depressed freezing point of these areas and so less time with frozen rock moisture present relative to areas with higher saturation.

The question of whether VE or IS is more important for frost weathering must be considered in a differentiated manner. Our experiments demonstrate that VE has the potential to cause the highest weathering intensity of all moisture-related processes; however, as the effects occur in short time windows, the more gradual effect of IS is most destructive overall (inferred from the higher number of AE events). A temperature dependence of IS shown in our findings and those of previous studies suggest a Fcw of −4°C to −9°C for Wetterstein limestone. These results, combined with further observations from our experiment showing rock weathering intensity following the frozen fringe during top down thawing, suggest that while having rock moisture already present in the pores is important during freeze–thaw cycles, the continued availability of rock moisture (at depth or in the surroundings) is equally important to facilitate weathering processes such as IS.

Further studies are required with greater cycle repetition and more samples to account for potential random effects caused by porosity structural heterogeneity on stresses. Also, the addition of AE sensors on the surface of a rock sample during different climatic cycles would ensure that the effects of wetting and drying at the surface are not missed due to AE signal dissipation with distance.

Acknowledgments

The authors wish to express their gratitude to the Electronics Workshop team at UBT for the development of instruments and Manfred Fischer for laboratory support. We also thank the anonymous reviewers for their helpful comments. Open Access funding enabled and organized by Projekt DEAL.

Funding

This study was supported by the Deutsche Forschungsgemeinschaft (DFG) [Project number 426793773].

Ethics Statement

The authors have nothing to report.

Conflicts of Interest

The authors declare no conflicts of interest.

Data Availability Statement

The data that support the findings of this study are available from the corresponding author upon reasonable request.

References

1. D. Draebing, T. Mayer, B. Jacobs, and S. T. McColl, "Alpine Rockwall Erosion Patterns Follow Elevation-Dependent Climate Trajectories," *Communications Earth & Environment* 3 (2022): 21, https://doi.org/10.1038/s43247-022-00348-2.

2. M. Rode, H. Schnepfleitner, and O. Sass, "Simulation of Moisture Content in Alpine Rockwalls During Freeze–Thaw Events," *Earth Surface Processes and Landforms* 41 (2016): 1937–1950, https://doi.org/10.1002/esp.3961.

3. B. D. Collins, G. M. Stock, M.-C. Eppes, et al., "Thermal Influences on Spontaneous Rock Dome Exfoliation," *Nature Communications* 9 (2018): 762. https://doi.org/10.1038/s41467-017-02728-1.

4. M. C. Eppes and R. Keanini, "Mechanical Weathering and Rock erosion by Climate-Dependent Subcritical Cracking," *Reviews of Geophysics* 55 (2017): 470–508, https://doi.org/10.1002/2017RG000557.

5. M. C. Eppes, "Mechanical Weathering: a Conceptual Overview," in *Treatise on Geomorphology*, vol. 3, ed. J. J. F. Shroder (Elsevier, 2022), 30–45, https://doi.org/10.1016/B978-0-12-818234-5.00200-5.

6. D. Draebing, M. Krautblatter, and T. Hoffman, "Thermo-Cryogenic Controls of Fracture Kinematics in Permafrost Rockwalls," *Geophysical Research Letters* 44 (2017): 3535–3544, https://doi.org/10.1002/2016GL072050.

7. M. C. Eppes, B. Magi, B. Hallet, et al., "Deciphering the Role of Solar-Induced Thermal Stresses in Rock Weathering," *Geological Society of America Bulletin* 128 (2016): 1315–1338, https://doi.org/10.1130/b31422.1.

8. H. J. M. Gage, J. P. Nielsen, and C. H. Eyles, "Temporal Variability and Site Specificity of Thermo-Mechanical Weathering in a Temperate Climate," *Frontiers in Earth Science* 12 (2024): 1318747, https://doi.org/10.3389/feart.2024.1318747.

9. K. Hall and M. F. André, "New Insights Into Rock Weathering as Deduced From High-Frequency Rock Temperature Data: an Antarctic Study," *Geomorphology* 41 (2001): 23–35.

10. T. Mayer, M. Eppes, and D. Draebing, "Influences Driving and Limiting the Efficacy of Ice Segregation in Alpine Rocks," *Geophysical Research Letters* 50 (2023): 2023GL102951, https://doi.org/10.1029/2023GL102951.

11. A. Mitchell and O. Sass, "Rock Weathering: The Effects of Varying Rock Moisture on Controlled Weathering Cycles in Low Porosity Limestone," *Geomorphology* 457 (2024): 109149, https://doi.org/10.1016/j.geomorph.2024.109149.

12. M. Offer, S. Weber, M. Krautblatter, I. Hartmeyer, and M. Keuschnig, "Pressurised Water Flow in Fractured Permafrost Rocks Revealed by Borehole Temperature, Electrical Resistivity Tomography, and Piezometric Pressure," *Cryosphere* 19 (2025): 485–506, https://doi.org/10.5194/tc-19-485-2025.

13. O. Sass, "Rock Moisture Measurements: Techniques, Results, and Implications for Weathering," *Earth Surface Processes and Landforms* 30 (2005): 359–374, https://doi.org/10.1002/esp.1214.

14. R. Scandroglio, V. Stoll, and M. Krautblatter, "The Driving Force of All Nature: Modelling Water Pressure and Its Stability Consequences on Alpine Bedrock Slopes," IOP Conference Series: Earth and Environmental Science, 833 (2021): 012109. https://doi.org/10.1088/1755-1315/833/1/012109.

15. P. Mamot, S. Weber, S. Eppinger, and M. Krautblatter, "A Temperature-Dependent Mechanical Model to Assess the Stability of Degrading Permafrost Rock Slopes," *Earth Surface Dynamics* 9 (2021): 1125–1151, https://doi.org/10.5194/esurf-9-1125-2021.

16. S. Kjelstrup, S. A. Ghoreishian Amiri, B. Loranger, H. Gao, and G. Grimstad, "Transport Coefficients and Pressure Conditions for Growth of Ice lens in Frozen Soil," *Acta Geotechnica* 16 (2021): 2231–2239, https://doi.org/10.1007/s11440-021-01158-0.

17. M. Maľa, V. Greif, and M. Ondrášik, "Pore Structure Evolution in Andesite Rocks Induced by Freeze-Thaw Cycles Examined by Non-Destructive Methods," *Scientific Reports* 12 (2022): 8390, https://doi.org/10.1038/s41598-022-12437-5.

18. O. Sass, "Rock Moisture Fluctuations During Freeze-Thaw Cycles: Preliminary Results From Electrical Resistivity Measurements," *Polar Geography* 28 (2004): 13–31, https://doi.org/10.1080/789610157.

19. K. Hall, "Mechanical Weathering in Cold Regions," in *Treatise on Geomorphology*, ed. J. F. Shroder (Academic Press, 2013), 258–276, https://doi.org/10.1016/B978-0-12-374739-6.00062-2.

20. D. L. Egholm, J. L. Andersen, M. F. Knudsen, J. D. Jansen, and S. B. Nielsen, "The Periglacial Engine of Mountain erosion—Part 2: Modelling Large-Scale Landscape Evolution," *Earth Surface Dynamics* 3 (2015): 463–482, https://doi.org/10.5194/esurf-3-463-2015.

21. T. C. Hales and J. J. Roering, "A Frost "Buzzsaw" Mechanism for erosion of the Eastern Southern Alps, New Zealand," *Geomorphology* 107 (2009): 241–253, https://doi.org/10.1016/j.geomorph.2008.12.012.

22. N. Matsuoka and J. Murton, "Frost Weathering: Recent Advances and Future Directions," *Permafrost & Periglacial* 19 (2008): 195–210, https://doi.org/10.1002/ppp.620.

23. N. Matsuoka, "A Multi-Method Monitoring of Timing, Magnitude and Origin of Rockfall Activity in the Japanese Alps," *Geomorphology* 336 (2019): 65–76, https://doi.org/10.1016/j.geomorph.2019.03.023.

24. K. Laute and A. A. Beylich, "Relating Ten Years of Rock Temperature Monitoring to Rockwall Weathering Processes in Steep Mountain Valleys in Western Norway," *Geomorphology* 468 (2025): 109496, https://doi.org/10.1016/j.geomorph.2024.109496.

25. B. Hallet, J. S. Walder, and C. W. Stubbs, "Weathering by Segregation Ice Growth in Microcracks at Sustained Sub-Zero Temperatures: Verification From an Experimental Study Using Acoustic Emissions," *Permafrost and Periglacial Processes* 2 (1991): 283–300, https://doi.org/10.1002/ppp.3430020404.

26. M. A. Perras and M. S. Diederichs, "A Review of the Tensile Strength of Rock: Concepts and Testing," *Geotechnical and Geological Engineering* 32 (2014): 525–546, https://doi.org/10.1007/s10706-014-9732-0.

27. S. Duca, C. Occhiena, M. Mattone, L. Sambuelli, and C. Scavia, "Feasibility of Ice Segregation Location by Acoustic Emission Detection: a

Laboratory Test in Gneiss," *Permafrost and Periglacial Processes* 25 (2014): 208–219, https://doi.org/10.1002/ppp.1814.

28. N. Matsuoka, "Microgelivation Versus Macrogelivation: Towards Bridging the Gap Between Laboratory and Field Frost Weathering," *Permafrost and Periglacial Processes* 12 (2001): 299–313, https://doi.org/10.1002/ppp.393.

29. J. S. Walder and B. Hallet, "The Physical Basis of Frost Weathering—Toward a More Fundamental and Unified Perspective," *Arctic and Alpine Research* 18 (1986): 27–32, https://doi.org/10.1080/00040851.1986.12004060.

30. O. Sass, "Spatial Patterns of Rockfall Intensity in the Northern Alps," *Zeitschrift für Geomorphologie Supplementband* 138 (2005): 51–65.

31. H. Jia, W. Xiang, and M. Krautblatter, "Quantifying Rock Fatigue and Decreasing Compressive and Tensile Strength After Repeated Freeze-Thaw Cycles," *Permafrost and Periglacial Processes* 26 (2015): 368–377.

32. D. Gerber, L. A. Wilen, F. Poydenot, E. R. Dufresne, and R. W. Style, "Stress Accumulation by Confined Ice in a Temperature Gradient," *Proceedings of the National Academy of Sciences of the United States of America* 119 (2022): e2200748119, https://doi.org/10.1073/pnas.2200748119.

33. D. N. Sibley, P. Llombart, E. G. Noya, A. J. Archer, and L. G. MacDowell, "How Ice Grows From Premelting Films and Water Droplets," *Nature Communications* 12 (2021): 239, https://doi.org/10.1038/s41467-020-20318-6.

34. T. Wang, Q. Sun, H. Jia, J. Ren, and T. Luo, "Linking the Mechanical Properties of Frozen Sandstone to Phase Composition of Pore Water Measured by LF-NMR at Subzero Temperatures," *Bulletin of Engineering Geology and the Environment* 80 (2021): 4501–4513, https://doi.org/10.1007/s10064-021-02224-3.

35. J. B. W. Webber, J. C. Dore, J. H. Strange, R. Anderson, and B. Tohidi, "Plastic Ice in Confined Geometry: the Evidence From Neutron Diffraction and NMR Relaxation," *Journal of Physics. Condensed Matter* 19 (2007): 415117, https://doi.org/10.1088/0953-8984/19/41/415117.

36. G. W. Scherer, "Crystallization in Pores," *Cement and Concrete Research* 29 (1999): 1347–1358, https://doi.org/10.1016/S0008-8846(99)00002-2.

37. F. Magnin and J. Y. Josnin, "Water Flows in Rock Wall Permafrost: a Numerical Approach Coupling Hydrological and Thermal Processes," *Journal of Geophysical Research - Earth Surface* 126 (2021): e2021JF006394, https://doi.org/10.1029/2021JF006394.

38. D. Draebing and T. Mayer, "Topographic and Geologic Controls on Frost Cracking in Alpine Rockwalls," *Journal of Geophysical Research - Earth Surface* 126 (2021): e2021JF006163, https://doi.org/10.1029/2021JF006163.

39. D. Lockner, "The Role of Acoustic Emission in the Study of Rock Fracture," *International Journal of Rock Mechanics and Mining Sciences* 30 (1993): 883–899, https://doi.org/10.1016/0148-9062(93)90041-B.

40. V. Maji and J. Murton, "Experimental Observations and Statistical Modeling of Crack Propagation Dynamics in Limestone by Acoustic Emission Analysis During Freezing and Thawing," *Journal of Geophysical Research: Earth Surface* 126 (2021): e2021JF006127, https://doi.org/10.1029/2021JF006127.

41. B. Goszczyńska, "Analysis of the Process of Crack Initiation and Evolution in Concrete With Acoustic Emission Testing," *Archives of Civil and Mechanical Engineering* 14 (2014): 134–143, https://doi.org/10.1016/j.acme.2013.06.002.

42. T. Mayer, M. Deprez, L. Schröer, V. Cnudde, and D. Draebing, "Quantifying Frost-Weathering-Induced Damage in Alpine Rocks," *Cryosphere* 18 (2024): 2847–2864, https://doi.org/10.5194/tc-18-2847-2024.

43. M. H. Loke, "Tutorial: 2D- and 3D-Electrical Imaging Surveys," 2001. Accessed September 17, 2025. https://www.researchgate.net/publication/264739285_Tutorial_2-D_and_3-D_Electrical_Imaging_Surveys.

44. O. Sass, "Moisture Distribution in Rockwalls Derived From 2D-Resistivity Measurements in Geophysical Applications in Geomorphology," *Zeitschrift Für Geomorphologie. Supplementband* 132 (2003): 51–69.

45. A. Schepers and H. Milsch. "Relationships Between Fluid-Rock Interactions and the Electrical Conductivity of Sandstones," *Journal of Geophysical Research: Solid Earth* 118 (2013): 3304–3317. Portico, https://doi.org/10.1002/jgrb.50241.

46. R. Killick, P. Fearnhead, and I. A. Eckley, "Optimal Detection of Changepoints With a Linear Computational Cost," *Journal of the American Statistical Association* 107 (2012): 1590–1598, https://doi.org/10.1080/01621459.2012.737745.

47. J. Teng, D. Antai, S. Zhang, X. Zhang, and D. Sheng, "Freezing-Thawing Hysteretic Behavior of Soils," *Water Resources Research* 60 (2024): e2024WR037280, https://doi.org/10.1029/2024WR037280.

48. I. Satoh, K. Fushinobu, and Y. Hashimoto, "Freezing of a Water Droplet due to Evaporation—Heat Transfer Dominating the Evaporation–Freezing Phenomena and the Effect of Boiling on Freezing Characteristics," *International Journal of Refrigeration* 25 (2002): 226–234, https://doi.org/10.1016/S0140-7007(01)00083-4.

49. S. Gruber and W. Haeberli, "Permafrost in Steep Bedrock Slopes and Its Temperature-Related Destabilization Following Climate Change," *Journal of Geophysical Research* 112 (2007): F02S18, https://doi.org/10.1029/2006JF000547.

50. S. K. Amankwah, A. M. Ireson, C. Maulé, R. Brannen, and S. A. Mathias, "A Model for the Soil-Freezing Characteristic Curve That Represents the Dominant Role of Salt Exclusion," *Water Resources Research* 57 (2021): e2021WR030070, https://doi.org/10.1029/2021WR030070.

51. MISTRAS Group. "Micro-SHM System Users Manual" 2017.

52. G. Manthei and M. Guckert, "Classification of Located Acoustic Emission Events Using Neural Network," *Journal of Nondestructive Evaluation* 42 (2023): 4, https://doi.org/10.1007/s10921-022-00913-x.

53. P. Hoekstra, "Moisture Movement in Soils Under Temperature Gradients With the Cold-Side Temperature Below Freezing," *Water Resources Research* 2 (1966): 241–250, https://doi.org/10.1029/wr002i002p00241.

54. D. H. Everett, "Thermodynamics of Frost Damage to Porous Solids," *Transactions of the Faraday Society* 57 (1961): 1541–1551, https://doi.org/10.1039/tf9615701541.

55. A. Lavrov, "The Kaiser Effect in Rocks: Principles and Stress Estimation Techniques," *International Journal of Rock Mechanics and Mining Sciences* 40 (2003): 151–171, https://doi.org/10.1016/S1365-1609(02)00138-7.

56. R. S. Anderson, "Near-Surface Thermal Profiles in Alpine Bedrock: Implications for the Frost Weathering of Rock," *Arctic and Alpine Research* 30 (1998): 362–372, https://doi.org/10.2307/1552008.

57. H. Wang, J. Ma, F. Du, G. Wang, Q. Zhang, and X. Li, "Research on the Attenuation Characteristics of AE Signals of Marble and Granite Stone," *Advances in Civil Engineering* 2020 (2020): 1–19, https://doi.org/10.1155/2020/6680347.

58. A. M. Al-Bared, I. S. H. Harahap, N. H. Azuddin, et al., "IOP Conf. Ser.: Earth Environmental Sciences, (2020);476:012040. https://doi.org/10.1088/1755-1315/476/1/012040.

59. M. Deprez, T. De Kock, G. De Schutter, and V. Cnudde, "The Role of Ink-Bottle Pores in Freeze-Thaw Damage of Oolithic Limestone," *Construction and Building Materials* 246 (2020): 118515, https://doi.org/10.1016/j.conbuildmat.2020.118515.

60. J. Dewanckele, M. A. Boone, T. De Kock, et al., "Holistic Approach of Pre-Existing Flaws on the Decay of Two Limestones," *Science of the*

Total Environment 447 (2013): 403–414, https://doi.org/10.1016/j.scitotenv.2012.12.094.

61. A. Voigtländer, "Controls of Progressive Rock Failure: Environmental Conditions, Subcritical Mechanisms and Rock Stress Memory. Dissertation. Technische Universität München," (2020):194. Accessed September 17, 2025. https://nbn-resolving.de/urn/resolver.pl?urn=nbn:de:bvb:91-diss-20201026-1551893-1-7.

62. Y. Israeli and S. Emmanuel, "Impact of Grain Size and Rock Composition on Simulated Rock Weathering," *Earth Surface Dynamics* 6 (2018): 319–327, https://doi.org/10.5194/esurf-6-319-2018.

63. F. Musso Piantelli, M. Herwegh, F. S. Anselmetti, M. Waldvogel, and U. Gruner, "Microfracture Propagation in Gneiss Through Frost Wedging: Insights From an Experimental Study," *Natural Hazards* 100 (2020): 843–860, https://doi.org/10.1007/s11069-019-03846-3.

64. V. Maji and J. Murton, "Experimental Observations That Simulated Active-Layer Deepening Drives Deeper Rock Fracture," *Permafrost and Periglacial Processes* 31, no. 2 (2020): 296–310.

65. A. Prick, "Critical Degree of Saturation as a Threshold Moisture Level in Frost Weathering of Limestones," *Permafrost and Periglacial Processes* 8 (1997): 91–99, https://doi.org/10.1002/(SICI)1099-1530(199701)8:1<91::AID-PPP238>3.0.CO;2-4.

66. T. C. C. Chen, M. R. R. Yeung, and N. Mori, "Effect of Water Saturation on Deterioration of Welded Tuff due to Freeze-Thaw Action," *Cold Regions Science and Technology* 38 (2004): 127–136, https://doi.org/10.1016/j.coldregions.2003.10.001.

67. J. Murton, R. Peterson, and J. C. Ozouf, "Bedrock Fracture by Ice Segregation in Cold Regions," *Science* 314 (2006): 1127–1129, https://doi.org/10.1126/science.1132127.

68. Q. Zhang, Y. Liu, G. He, Q. Chen, X. Ou, and J. Tian, "Study on the Effects of Different Water Content Rates on the Strength and Brittle Plasticity of Limestone," *Applied Sciences* 13 (2023): 4685, https://doi.org/10.3390/app13084685.

69. J. Walder and B. Hallet, "A Theoretical-Model of the Fracture of Rock During Freezing," *Geological Society of America Bulletin* 96 (1985): 336–346, https://doi.org/10.1130/0016-7606.

70. M. Deprez, T. De Kock, G. De Schutter, and V. Cnudde, "A Review on Freeze-Thaw Action and Weathering of Rocks," *Earth Science Reviews* 203 (2020): 103143, https://doi.org/10.1016/j.earscirev.2020.103143.

71. I. Vlahou and M. G. Worster, "Freeze Fracturing of Elastic Porous Media: a Mathematical Model," *Proceedings of the Royal Society A: Mathematical, Physical and Engineering Sciences* 471, no. 2175 (2015): 20140741, https://doi.org/10.1098/rspa.2014.0741.

72. O. Borgman, P. Fantinel, W. Lühder, L. Goehring, and R. Holtzman, "Impact of Spatially Correlated Pore-Scale Heterogeneity on Drying Porous Media," *Water Resources Research* 53 (2017): 5645–5658, https://doi.org/10.1002/2016WR020260.

73. H. Luo, D. Jougnot, A. Jost, J. Teng, and L. D. Thanh, "A Capillary Bundle Model for the Electrical Conductivity of Saturated Frozen Porous Media," *Journal of Geophysical Research: Solid Earth* 128 (2023): e2022JB025254, https://doi.org/10.1029/2022JB025254.

74. T. De Kock, M. A. Boone, T. De Schryver, et al., "A Pore-Scale Study of Fracture Dynamics in Rock Using X-Ray Micro-CT Under Ambient Freeze–Thaw Cycling," *Environmental Science & Technology* 49 (2015): 2867–2874, https://doi.org/10.1021/es505738d.

75. B. Ghanbarian and H. Daigle, "Thermal Conductivity in Porous Media: Percolation-Based Effective-Medium Approximation," *Water Resources Research* 52 (2015): 295–314, https://doi.org/10.1002/2015WR017236.

76. X. Li, K. Peng, J. Peng, and D. Hou, "Experimental Investigation of Cyclic Wetting-Drying Effect on Mechanical Behavior of a Medium-Grained Sandstone," *Engineering Geology* 293 (2021): 106335, https://doi.org/10.1016/j.enggeo.2021.106335.

77. D. Draebing and M. Krautblatter, "The Efficacy of Frost Weathering Processes in Alpine Rockwalls," *Geophysical Research Letters* 46 (2019): 6516–6524, https://doi.org/10.1029/2019GL081981.

78. N. Matsuoka, "Mechanisms of Rock Breakdown by Frost Action: an Experimental Approach," *Cold Regions Science and Technology* 17 (1990): 253–270, https://doi.org/10.1016/S0165-232X(05)80005-9.

79. Z. Fu, Q. Wu, W. Zhang, H. He, and L. Wang, "Water Migration and Segregated Ice Formation in Frozen Ground: Current Advances and Future Perspectives," *Frontiers in Earth Science* 10 (2022): 826961, https://doi.org/10.3389/feart.2022.826961.

80. T. C. Hales and J. J. Roering, "Climatic Controls on Frost Cracking and Implications for the Evolution of Bedrock Landscapes," *Journal of Geophysical Research* 112 (2007): F02033, https://doi.org/10.1029/2006JF000616.

81. A. W. Rempel, J. A. Marshall, and J. J. Roering, "Modeling Relative Frost Weathering Rates at Geomorphic Scales," *Earth and Planetary Science Letters* 453 (2016): 87–95, https://doi.org/10.1016/j.epsl.2016.08.019.

82. L. Girard, S. Gruber, S. Weber, and J. Beutel, "Environmental Controls of Frost Cracking Revealed Through in Situ Acoustic Emission Measurements in Steep Bedrock," *Geophysical Research Letters* 40 (2013): 1748–1753, https://doi.org/10.1002/grl.50384.

83. M. Wegmann, "Frostdynamik in hochalpinen Felswänden am Beispiel der Region Jungfraujoch-Aletsch. Mitteilungen No. 161 der Versuchsanstalt für Wasserbau, Hydrologie und Glaziologie. ETH-Zentrum, Zürich," (1998): 37–39.

84. M. G. Wolman and J. P. Miller, "Magnitude and Frequency of Forces in Geomorphic Processes," *Journal of Geology* 68 (1960): 54–74, https://doi.org/10.1086/626637.

85. P. Guo, "Dependency of Tortuosity and Permeability of Porous Media on Directional Distribution of Pore Voids," *Transport in Porous Media* 95 (2012): 285–303, https://doi.org/10.1007/s11242-012-0043-8.

86. T. R. Zakirov and M. G. Khramchenkov, "Prediction of Permeability and Tortuosity in Heterogeneous Porous Media Using a Disorder Parameter," *Chemical Engineering Science* 227 (2020): 115893, https://doi.org/10.1016/j.ces.2020.115893.

87. A. Sekerbayeva, A. Mortazavi, R. D. Hazlett, and B. Bohloli, "Fault Gouge Permeability Under Confined Conditions: an Investigation for CO_2 Storage Applications," *Energies* 18 (2025): 9, https://doi.org/10.3390/en18010009.

88. J. P. Coutard and B. Francou, "Rock Temperature Measurements in Two Alpine Environments: Implications for Frost Shattering," *Arctic and Alpine Research* 21 (1989): 399–416, https://doi.org/10.2307/1551649.

Supporting Information

Additional supporting information can be found online in the Supporting Information section. Temperature range of freezing points determined by temperature isotherm and sharp moisture decrease is shown in Figure S1. From Figures S2 to S6, cumulative rock moisture movement during different processes seen at depth across cycles in short, diurnal cycles and long, ca.72-h cycles is displayed. Finally, average change in wave speed velocity of AE events when the rock moisture is in frozen and unfrozen state is shown in Figure S7. **FIGURE S1:** Freezing point of rock moisture determined by abrupt drop in electrical conductivity and latent heat isotherms in temperature data. exp.75 (blue), exp.70 (orange), exp.60 (green) and exp.50 (purple). 0°C line shown by dashed line. **FIGURE S2:** Cumulative rock moisture movement due to capillary rise seen across cycles in short, diurnal cycles (blue) and long, ca.72-h cycles (orange). Depth from sample surface in centimetres. **FIGURE**

S3: Cumulative rock moisture movement due to cryosuction to surface seen across cycles in short, diurnal cycles (blue) and long, ca.72-h cycles (orange). Depth from sample surface in centimetres. **FIGURE S4:** Cumulative rock moisture movement due to frozen decrease in liquid rock moisture, due to phase change during freezing, seen across cycles in short, diurnal cycles (blue) and long, ca.72-h cycles (orange). Depth from sample surface in centimetres. **FIGURE S5:** Cumulative rock moisture movement due to frozen increase of rock moisture seen due to phase during thawing change across cycles in short, diurnal cycles (blue) and long, ca.72-h cycles (orange). Depth from sample surface in centimetres. **FIGURE S6:** Cumulative rock moisture movement due to cryosuction to base seen during thawing across cycles in short, diurnal cycles (blue) and long, ca.72-h cycles (orange). Depth from sample surface in centimetres. **FIGURE S7:** Average wave speed velocity used in AE event linear interpolation for each experiment when rock moisture in frozen and unfrozen state.